Freezing of binary mixtures of colloidal hard spheres

P. Bartlett and R. H. Ottewill
School of Chemistry, Bristol University, Bristol, BS8 1TS, England

P. N. Pusey
Royal Signals and Radar Establishment, Malvern, WR14 3PS, England

(Received 5 January 1990; accepted 19 March 1990)

The freezing phase transition in a binary suspension of colloidal hard spheres of diameter ratio $\alpha = 0.61$ was studied by light scattering and scanning electron microscopy. The suspensions consisted of sterically stabilized poly(methyl methacrylate) spheres of diameters about 670 and 407 nm suspended in a near refractive indexed matched suspension medium composed of carbon disulphide and *cis*-decalin. With increasing volume fraction, binary suspensions of number fraction of larger component A $x_A > 0.43$ crystallized to give irregularly stacked close packed crystals containing almost entirely component A. As the number fraction x_A decreased, the rate of crystallization decreased. Suspensions of $x_A \approx 0.28$ remained amorphous and showed glassy behavior. Suspensions of $x_A \approx 0.057$ showed a complex sequence of phase behavior with coexistence of crystals of component B, the ordered binary alloy phase AB_{13}, and a binary fluid. In suspensions with $x_A < 0.057$, the only solid phase observed was irregularly stacked close packed crystals of component B. The observed phase behavior is compared with the predictions of a model for freezing of a mixture of hard spheres which are assumed to be immiscible in the solid phase.

I. INTRODUCTION

Suspensions of monodisperse colloidal particles are known to undergo a freezing transition from a disordered fluid phase to an ordered crystal structure with an increase in particle volume fraction. The aim of the present work is to investigate experimentally this fluid–solid phase transition in a binary mixture of colloids (diameter ratio $\alpha = 0.61 \pm 0.02$) for which the interparticle potential is steeply repulsive and closely approximated by a hard sphere interaction. The freezing of liquids made up of atoms which interact through a hard sphere potential has been extensively studied by computer simulation.[1] Although less attention has been paid to the more complex case of the freezing of binary mixtures, a mixture of hard spheres provides a natural reference state from which to interpret the observed variety of binary phase diagrams.

Binary hard sphere mixtures of all diameter ratios α are expected to be completely miscible in the fluid phase.[2] By contrast, simple packing arguments suggest the composition and structure of the equilibrium solid phase is determined primarily by the size ratio α. Density functional calculations[3] suggest that spheres of comparable diameters crystallize into disordered face-centered-cubic (fcc) structures. As the diameter ratio α decreases the degree of mutual solubility decreases and the phase diagram changes from a spindle shape to an azeotropic diagram and finally into a eutectic diagram. At the most extreme size ratio reported[3] of $\alpha = 0.85$, the solid phase separation results in a pure fcc crystal of small spheres and a substitutionally disordered fcc crystal containing largely big spheres. Spheres of smaller diameter ratios can form ordered binary alloy structures. For example, if the larger spheres form a close packed fcc structure, then there are octahedral interstitial holes that can accomodate spheres of diameter ratio $\alpha \leqslant \sqrt{2} - 1$ and tetrahedral holes of diameter ratio $\frac{1}{2}\sqrt{6} - 1$. A simple free volume argument suggests binary structures with close packed densities in excess of the close packed volume fraction for monodisperse spheres of $\varphi = 0.7405$ should be preferred at least at high pressures. Although the structures formed at freezing are not close packed (in the sense that the particles are not touching), it seems reasonable to expect similar structures will be important. Sanders and Murray[4] have calculated the close packed densities of a wide range of binary alloy structures. With decreasing size ratio, the number of potential structures increases rapidly, but for $\alpha \geqslant \sqrt{2} - 1$ high density close packed binary alloys are found for size ratios of $\alpha = 0.566$ (cubic AB_{13}, $\varphi = 0.760$), $\alpha = 0.527$ (hexagonal AB_2, $\varphi = 0.782$), and $\alpha = 0.414$ (cubic AB, $\varphi = 0.793$). Rather surprisingly, recent density functional calculations[5] of the freezing of hard sphere mixtures (1:1 number ratio) predict that the stable solid phase at freezing for all size ratios is the disordered fcc structure. In binary systems of small size ratios, partially frozen crystal structures are geometrically possible. In such structures, the larger component is localized, while the smaller second component is free to diffuse throughout the crystal lattice. Computer simulation studies[6] have shown that a diameter ratio no larger than 0.4 can be tolerated in a fcc lattice without both components becoming either localized or fluid.

The similarity of concentrated colloidal suspensions to simple liquids makes them ideal candidates to test experimentally both equilibrium and nonequilibrium theories of the condensed phase. If the suspension medium is regarded as a continuous background, a colloidal suspension is thermodynamically equivalent to a system of interacting particles,[7,8] in which the interparticle potential (or strictly the potential of mean force) implicitly includes all solvent corre-

 0021-9606/90/141299-14$03.00

lations. As systems for experimental study, particle suspensions have several advantages compared with simple liquids. Binary suspensions of almost any size ratio may be studied since particles can by synthesized with a wide range of particle sizes.[9] Nonequilibrium processes such as glass formation[10] and shear-induced order,[11] which are not readily observable in simple liquids, may be studied in a colloidal suspension as a result of the long relaxation time for particle diffusive motion. Experimental observation is greatly facilitated by the large interparticle spacing. Structural information may be derived from light scattering, electron microscopy, or in favorable cases directly from optical microscopy.[12]

The colloidal particles used in the present work consisted of a poly(methyl methacrylate) (PMMA) core coated by a covalently grafted outer layer of a comb polymer, poly(12-hydroxy stearic acid) (PHS) dispersed in a refractive index matching mixture of carbon disulphide and cis-decalin. Nearly transparent suspensions at high number densities can be prepared allowing detailed studies by light scattering. This is a well-characterized model colloidal system which has been used in a range of previous studies.[10,11,13–17] In a nonpolar medium, electrostatic effects should be negligible, while the attractive interparticle (van der Waals) forces are expected to be minimized by matching the medium and particle refractive indices. Consequently the interparticle potential should be purely repulsive arising only from the compression of the densely packed grafted chains. While the precise magnitude of the steric repulsive potential is uncertain, the distance dependence of the interaction between terminally attached polymer layers in a good solvent has been predicted by scaling arguments[18] and is in close agreement with direct force measurements.[19] Both theory and experiment show the interaction potential to be steeply repulsive and insignificant when the surfaces of the core particles are separated by more than twice the mean thickness of the grafted layer. The steepness of the interparticle repulsive potential may be estimated from the measured mean thickness ($\approx$10 nm) of the PHS layer[16] and the estimated mean distance between PHS anchor points ($\approx$3 nm). For a sphere of radius 200 nm, the interparticle potential is negligible for a surface-to-surface separation greater than 20 nm and predicted to be of the order of 10 kT for surface separations of 17–18 nm. This is in approximate agreement with osmotic pressure measurements made on this system.[13] While there is some evidence for the interaction potential between small PMMA particles to be slightly "soft,"[16] all measurements reported below were made on particles with radii greater than 200 nm and in this case the potential curve should be closely approximated by a hard sphere interaction.

The assumption of a hard sphere interaction is supported by a variety of experimental evidence. Earlier studies[15] of similar particles have shown that a concentrated one component suspension shows, with increasing concentration, the full range of phase behavior, predicted for a hard sphere system, of colloidal fluid, colloidal crystal, and colloidal glass. Static light scattering measurements[14] have established that the osmotic compressibility closely follows the predictions of the Percus–Yevick equation of state for hard spheres. A detailed analysis[17] of the scattering from the colloidal crystal phase is consistent with the very small energy difference between face-centered-cubic and hexagonal close packing predicted by computer simulations[20] of hard spheres.

Ordered alloy structures have been observed previously in aqueous binary mixtures of colloidal polystyrene spheres.[12] In contrast to the work reported here, the polystyrene spheres interact through a long range (soft) screened Coulombic potential. Optical microscopy was used to determine the alloy structures formed in the turbid suspensions, so observations were limited to near cell walls where surface effects could well be important.

This paper is organized as follows: In Sec. II, we discuss sample preparation, scanning electron microscopy, and light scattering measurements. The experimental phase behavior found in binary suspensions is described in Sec. III. In Sec. IV, the phase behavior of a mixture of hard spheres, which are assumed to be totally immiscible in the solid phase, is calculated from accurate statistical equations of state. The calculated fluid–solid phase equilibria are presented in a form appropriate for direct comparison with our constant volume measurements, reported in Sec. III. In addition, we discuss how the phase equilibria in an experimental system might be expected to deviate from the calculations in the vicinity of a eutectic. In Sec. V, we compare our experimental results with the predictions of this simple model.

II. EXPERIMENTAL DETAILS

A. Sample preparation

Colloidal PMMA particles were synthesized by a one step dispersion polymerization[9] using methods previously described. Transmission electron microscopy, dynamic light scattering,[21] and light crystallography were used to determine the number average particle diameters and their polydispersities (standard deviation divided by the mean size). The results are listed in Table I. Although there is a slight variation in the mean diameter between different measurements, the diameter ratio is fairly constant at 0.61 ± 0.02.

Colloidal suspensions were prepared using a mixture of *cis*-decalin and carbon disulphide (CS_2 mass fraction 0.245) whose composition was adjusted to match the mean particle refractive index of 1.508 at a wavelength of 568.2 nm and 22.0 °C. Although carbon disulphide is adsorbed preferentially in the PMMA core,[22] the consequent increase in particle radius is relatively small. Measurement by light scatter-

TABLE I. Number average diameters of colloidal particles and their polydispersities determined from transmission electron microscopy (TEM), dynamic light scattering (DLS), and light crystallography (LC) measurements.

System	Diameter (nm)			Polydispersity	
	TEM	DLS	LC	TEM	DLS
Component *A*	648 ± 32	670 ± 10	641 ± 6	4.0%	2.8%
Component *B*	430 ± 22	407 ± 10	398 ± 6	5.4%	4.8%
Diameter ratio α	0.66 ± 0.05	0.61 ± 0.02	0.62 ± 0.01		

TABLE II. Experimentally determined core volume fractions at freezing (φ_f^c) and melting (φ_m^c) for suspensions of colloidal components A and B. The scaled volume fractions correspond to an effective hard sphere diameter of $\sigma_{\text{eff}} = \sigma_{\text{core}} + 2\Delta r$, where σ_{eff} is given in Table I and Δr is the effective adsorbed layer thickness given below.

System	Core volumes		Scaled volumes		
	φ_f^c	φ_m^c	φ_f	φ_m	Δr (nm)
Component A	0.419 ± 0.005	0.463 ± 0.005	0.494	0.545 ± 0.006	18.9 ± 1.4
Component B	0.407 ± 0.005	0.448 ± 0.005	0.494	0.543 ± 0.006	13.6 ± 0.9

ing of the radius of gyration of component A as a function of medium refractive index (for a description of the theory see Ref. 23) indicated that the geometric particle radius increased by less than 3% in the carbon disulphide/decalin suspension medium. As a result of this swelling by carbon disulphide, and because of incomplete characterization of the PHS coating, it is impossible to calculate reliably the suspension volume fraction. As in previous studies,[15] the interparticle potential is assumed to be hard sphere and the concentration at which crystallization of each pure component first occurred was identified with a hard sphere volume fraction of 0.494, as determined by computer simulations.[24] All other concentrations were scaled by the same factor to provide effective hard sphere volume fractions. The volume fraction of the crystal phase at melting was identified with the lowest suspension concentration at which the equilibrium crystal phase fully occupied the cuvette. The concentration or core volume fraction of PMMA in the suspensions was calculated from mass measurements using literature values for the component densities. In Table II, the experimentally determined core volume fraction (φ_f^c) of the fluid phase at crystallization and the volume fraction of the crystal phase at melting (φ_m^c) are listed together with the resulting scaled freezing (φ_f) and melting (φ_m) effective hard sphere volume fractions for each component. The difference between the total volume fraction and the core volume fraction may be attributed to an effective adsorbed layer thickness Δr. Table II shows that the effective adsorbed layer thickness is slightly in excess of the mean adsorbed layer thickness of 10 nm determined by small angle neutron scattering measurements.[16] This difference probably reflects the extent of the swelling of the PMMA core due to penetration of carbon disulphide. Calculations for inverse power potentials[1] have shown that the fractional volume change upon melting is a very sensitive function of the steepness of the repulsive potential. The close agreement between the melting volume fraction given in Table II and the computer simulation result for hard spheres[24] of 0.545 supports the assumption of a steeply repulsive potential.

Optically matched binary suspensions were prepared by adding a weighed amount of a suspension in *cis*-decalin ($\varphi \approx 0.3$) of each component into a 1 cm square cross-section optical cuvette. A weighed quantity of carbon disulphide was added to match approximately the refractive index of the latex particles. The sample was then concentrated by centrifuging at 2000 g for at least five hours and the subsequent removal of a measured mass of supernatant. Redispersal of the particles by extensive tumbling (≈ 0.2 Hz) provided the desired concentrated suspensions. With careful sealing of the cuvette, evaporation of volatile carbon disulphide was negligible over a period of several months.

The binary suspension was characterized by the overall number fraction x_A of larger spheres and the overall total volume fraction φ, or if appropriate by the volume fractions φ_A and φ_B of each component

$$\varphi = \varphi_A + \varphi_B = \frac{\pi}{6}(\rho_B \sigma_B^3 + \rho_A \sigma_A^3), \quad x_A = \frac{\rho_A}{\rho_A + \rho_B}, \tag{1}$$

where ρ_i is the number density of component i and σ_i the particle diameter. Subscripts l and s refer to the fluid and solid phases, respectively, where a distinction is made between the overall volume fraction φ and the volume fraction of constituent phases (φ_l and φ_s). Samples were prepared at 13 different number fractions x_A spanning the composition range from $x_A = 0$ (pure component B) to $x_A = 1$ (pure component A). At each composition, samples were prepared with a range of total volume fractions chosen to span the region of fluid/solid coexistence. A total of 35 samples was prepared.

B. Crystallization

Light scattering measurements made on suspensions immediately after tumbling indicated that the particles were homogeneously randomized consistent with a degree of short range order, i.e., they were in an equilibrium or metastable fluid state. In single component suspensions of concentration in excess of the freezing density φ_f, small (homogeneously nucleated) Bragg reflecting crystallites formed throughout the bulk of the sample. For $\varphi_f < \varphi < \varphi_m$, the crystallites settled under gravity as a consequence of the higher density of the crystalline phase compared with that of the coexisting fluid phase and a well-defined boundary between the solid and coexisting fluid phase developed. From the height of this boundary, the equilibrium volumes of the solid (V_s) and fluid phases (V_l) were determined. The phase volume of the solid phase (η_s) is defined by $\eta_s = V_s/V_s + V_l$. In single component suspensions, the phase rule ensures that at equilibrium the solid sediment must be a single homogeneous phase. In binary systems, the additional degree of freedom removes this constraint and a solid sediment, which remains in equilibrium with a fluid phase, may consist of up to two distinct solid phases. In our experiments, the relative volume of each solid phase is not distinguished. The measured solid phase volume η_s refers to the total volume of all the high density solid phases which separate under

gravity from a coexisting single fluid phase. Experimental observations discussed in Sec. III indicate that under certain conditions the solid sediment formed from a crystallizing binary suspension consists of both crystalline and amorphous phases.

In contrast to single component systems in which crystallization, within the phase coexistence region, was essentially complete within a few days, the crystallization of binary samples was appreciably slower. In extreme cases, the gravitational sedimentation velocity of a crystal nucleus, or even the individual particles, may become comparable to the growth velocity of the crystallite–fluid interface. In such a case, gravitational settling dominates the observed phase behavior and dense amorphous sediments are found, often with a crystalline phase above (see Ref. 25 for a discussion of the analogous behavior observed in single component suspensions). The effects of gravity may be greatly reduced by a slow rotation of the samples in a vertical plane, so the time-averaged vertical sedimentation velocity of a particle relative to the suspension is zero. In effect the samples are subjected to (time averaged) zero gravity conditions. At an angular frequency of $\omega = 2\pi$ rad day^{-1}, samples remained homogeneous and crystallization proceeded throughout the sample volume. At any point, the sample could be subjected to "normal" gravity forces by stopping the rotation so that solid and fluid phases separated.

Continuous rotation of the sample imposes a roughly constant strain rate $\dot{\gamma}$ upon the suspension. By considering planes of particles perpendicular to the rotating radius vector, the strain rate $\dot{\gamma}$ is seen to be comparable to the angular frequency ω. The relative importance of an applied strain rate $\dot{\gamma}$ and Brownian diffusion in determining the equilibrium structure may be gauged from the magnitude of the dimensionless Peclet number $\mathrm{Pe} = \dot{\gamma}\tau_r$, where τ_r is a Brownian diffusion relaxation time. The relaxation time corresponds to the time for self-diffusion over a distance comparable to the particle radius and is given as $\tau_r = \sigma^2/24\,D_s$ ($\approx 4s$ in our system), where σ is the particle diameter and D_s is its self-diffusion constant. Insignificant distortion of the equilibrium structure occurs for $\mathrm{Pe} \ll 1$, where Brownian motion dominates shear forces. For our system, the estimated Peclet number is less than 10^{-3}, so that the equilibrium structure should be negligibly perturbed by slow rotation. This is in agreement with the experimental observation that slow tumbling does not alter significantly the equilibrium phase volumes for samples where cystallization is rapid and hence unaffected by gravitional settling.

C. Light scattering

Light scattering studies of the suspension structure were made using an automated diffractometer with an angular resolution of $\approx 0.25°$. Samples were mounted in the center of a cylindrical index matched bath of decalin–tetralin (refractive index ≈ 1.52) held at a constant temperature of 22.0 ± 0.1 °C. An expanded krypton ion laser beam illuminated a scattering volume of approximately 1 cm^3, typically containing in excess of 10^6 randomly orientated cystallites. Scattered light was focused by the cylindrical bath onto vertical slits placed in front of a photomultiplier. The photomultiplier was mounted on a computer controlled turntable and angular scans were made from a scattering angle of $2\vartheta = 20°$ to 140° in steps of 0.25°. The magnitude of the scattered wave vector, given by $q = (4\pi n/\lambda)\sin\vartheta$, was determined from the laser wavelength (λ) and the measured suspension refractive index (n). Each experiment lasted approximately 10 min.

Difficulty in the accurate determination of the zero of the angular scale introduces a systematic error into the angular position of the diffracted beam. For a cubic crystal, the angular error $\Delta\vartheta$ results in an uncertainity in the lattice spacing of Δa given by

$$\Delta a = \frac{a}{\tan\vartheta}\,\Delta\vartheta. \tag{2}$$

This systematic error was minimized by extrapolating the measured lattice parameter, from each sharp reflection, to $1/\tan\vartheta = 0$.

D. Scanning electron microscopy

In a few representative samples, the structure of the colloidal solid phase was studied by scanning electron microscopy. After the separation of the solid and fluid phases was complete, the colloidal fluid was carefully removed with a Pasteur pipette. The remaining solid phase was dried by allowing the suspension medium to evaporate naturally over a period of several months. The dried solid material was sputter coated with a thin film (≈ 15 nm thick) of gold and viewed directly in a Hitachi S-2300 microscope. Correlation of the observed structures with the results of light scattering measurements suggested that in the majority of cases this procedure produced little disruption of the colloidal structures initially present.

III. RESULTS

In Table III, the measured freezing data for the binary suspensions are listed in order of decreasing number fraction x_A of the overall sample. Samples were slow tumbled ($\omega \approx 1 \times 10^{-5}$ Hz) for total periods of up to three months and regular observations were made to check the approach to the equilibrium (metastable) lattice parameters (equal to $\sqrt{2}$ times the particle center-to-center separation).

Measurement of the scattering from the samples at equilibrium showed four distinct types of fluid–solid phase behavior. The approximate positions of the boundaries delineating the behaviors are represented by the dotted lines of constant number fraction x_A in the φ_A, φ_B plane of Fig. 1. (In Figs. 3–6, scattered intensity profiles from typical samples, characteristic of each region of phase behavior, are given. We shall consider each in detail.)

A. Region I

For $x_A \gtrsim 0.43$, all samples of sufficiently high total volume fraction showed colloidal crystal formation except for the highest density sample (25) which remained glassy and did not crystallize during our experiments. The rate of crystallization was observed to decrease rapidly as the initial number fraction x_A was reduced from unity and approached $x_A = 0.43$, although a quantitative study of crystallization rates was not made.

TABLE III. Freezing data for suspensions of colloidal hard sphere components and their mixtures. The quantity η_s is the fractional sample volume occupied by the solid phases, a_{obs} and a_{calc} are the measured and predicted equivalent fcc lattice parameters.

Sample number	Suspension details				Observed phase behavior			Predicted phase behavior		
	x_A	ϕ	ϕ_A	ϕ_B	η_s	a_{obs} (nm)	Phases present[a]	η_s	a_{calc} (nm)	Phases present[a]
8	1.00	0.523	0.523	0.000	0.56	1004	A + fluid	0.56	1004	A + fluid
30	0.934	0.543	0.536	7.78×10^{-3}	0.80	986	A + fluid	0.64	991	A + fluid
28	0.921	0.545	0.534	1.04×10^{-2}	0.75	···	···	0.61	988	A + fluid
29	0.885	0.546	0.530	1.56×10^{-2}	0.72	···	···	0.56	984	A + fluid
27	0.795	0.545	0.515	3.01×10^{-2}	0.57	976	A + fluid	0.46	977	A + fluid
34	0.732	0.548	0.506	4.21×10^{-2}	0.55	974	A + fluid	0.44	972	A + fluid
35	0.659	0.534	0.478	5.61×10^{-2}	0.40	972	A + fluid	0.29	971	A + fluid
33	0.660	0.545	0.488	5.70×10^{-2}	0.48	···	···	0.37	968	A + fluid
36	0.660	0.553	0.495	5.80×10^{-2}	0.64	969	A + fluid	0.43	965	A + fluid
37	0.659	0.562	0.503	5.89×10^{-2}	0.87	965	A + fluid	0.49	963	A + fluid
38	0.660	0.569	0.509	5.97×10^{-2}	0.92	962	A + fluid	0.53	961	A + fluid
59	0.578	0.536	0.460	7.63×10^{-2}	0.56	964	A + fluid	0.27	965	A + fluid
60	0.576	0.549	0.470	7.86×10^{-2}	0.70	959	A + fluid	0.36	961	A + fluid
61	0.582	0.563	0.484	7.90×10^{-2}	0.84	958	A + fluid	0.45	958	A + fluid
62	0.579	0.589	0.504	8.30×10^{-2}	1.00	949	A	0.57	950	A + fluid
26	0.437	0.496	0.384	0.112	0.00	···	Fluid	0.00	···	Fluid
20	0.446	0.512	0.400	0.113	0.65	955	A + fluid	0.04	962	A + fluid
21	0.437	0.534	0.413	0.121	0.38	947	A + fluid	0.20	956	A + fluid
23	0.437	0.550	0.425	0.125	0.71	948	A + fluid	0.31	952	A + fluid
25	0.440	0.622	0.482	0.139	1.00	···	Glassy	0.62	932	A + fluid
55	0.282	0.481	0.305	0.177	0.00	···	Fluid	0.00	···	Fluid
56	0.280	0.503	0.317	0.186	0.00	···	Fluid	0.00	···	Fluid
57	0.281	0.540	0.342	0.199	1.00	···	Glassy	0.20	944	A + fluid
58	0.280	0.553	0.350	0.204	1.00	···	Glassy	0.26	941	A + fluid
51	5.69×10^{-2}	0.481	0.101	0.380	0.00	···	Fluid	0.00	···	Fluid
52	5.66×10^{-2}	0.511	0.107	0.404	0.35	624	B + fluid	0.00	···	Fluid
53	5.63×10^{-2}	0.535	0.111	0.424	0.85	621[b]	AB_{13} + B + fluid	0.001(A) 0.13(B)	929(A) 619(B)	A + B + fluid[c]
54	5.68×10^{-2}	0.553	0.116	0.437	1.00	615	B	0.07(A) 0.41(B)	929(A) 619(B)	A + B + fluid[c]
63	3.03×10^{-2}	0.544	6.57×10^{-2}	0.478	1.00	615	B	0.01(A) 0.49(B)	929(A) 619(B)	A + B + fluid[c]
64	3.00×10^{-2}	0.551	6.61×10^{-2}	0.485	1.00	613	B	0.03(A) 0.61(B)	929(A) 619(B)	A + B + fluid[c]
31	3.03×10^{-2}	0.566	6.85×10^{-2}	0.497	1.00	611	B	0.09(A) 0.84(B)	929(A) 619(B)	A + B + fluid[c]
65	3.02×10^{-2}	0.577	6.95×10^{-2}	0.507	1.00	600	B	0.10(A) 0.90(B)	928(A) 616(B)	A + B[d]
66	3.01×10^{-2}	0.591	7.11×10^{-2}	0.520	1.00	591	B	0.10(A) 0.90(B)	926(A) 611(B)	A + B[d]
32	1.53×10^{-2}	0.563	3.61×10^{-2}	0.527	1.00	610	B	0.05(A) 0.95(B)	929(A) 619(B)	A + B[d]
17	0.000	0.508	0.000	0.508	0.26	623	B + fluid	0.26	623	B + fluid

[a] See the discussion in Sec. III for phase identification.

[b] Face centered cubic lattice parameter of coexisting AB_{13} crystal (space group $Fm3c$) is 1973 nm.

[c] Predicted to lie in the three phase region of the phase diagram. Equilibrium between the eutectic fluid of composition $\phi_A = 0.127$, $\phi_B = 0.405$, crystal A (lattice parameter 929 nm), and crystal B (lattice parameter 619 nm).

[d] Predicted to lie in the region of two phase solid equilibrium. The lattice parameters of the two solid phases crystal A and crystal B are given.

A scanning electron micrograph [Fig. 2(a)] of the dried solid phase of sample 33, $x_A = 0.660$, $\varphi = 0.545$ shows it to consist of large close packed regions of component A. Occluded B spheres were present only in amorphous grain boundaries. The solubility of component B in the crystal of component A was estimated from similar micrographs to be less than 1% for all samples with $x_A \geqslant 0.43$. These observations are consistent with almost total solid immiscibility of components A and B. As a consequence of this phase separation, the coexisting fluid phase will be enriched in component B. This was confirmed by the analysis of the coexisting fluid phase in sample 33. After the sample has reached equilibrium, the colloidal fluid was carefully removed from the solid phase. The fluid phase was then diluted with suspension medium and allowed to dry before a carbon replica was prepared. This was viewed directly by transmission electron microscopy. The equilibrium number fraction was estimated from the number of large spheres found in a random sample of approximately 3000 particles as $x_A = 0.59 \pm 0.03$. This is in close agreement with the equilibrium fluid composition $x_A = 0.51$ calculated for the freezing of mutually immiscible hard spheres and described in detail in Sec. IV. Thus, for $x_A \geqslant 0.66$, suspensions at concentrations between freezing and melting separate into a single crystalline A phase and a fluid phase enriched in component B.

Electron micrographs of the dried solid phase formed in

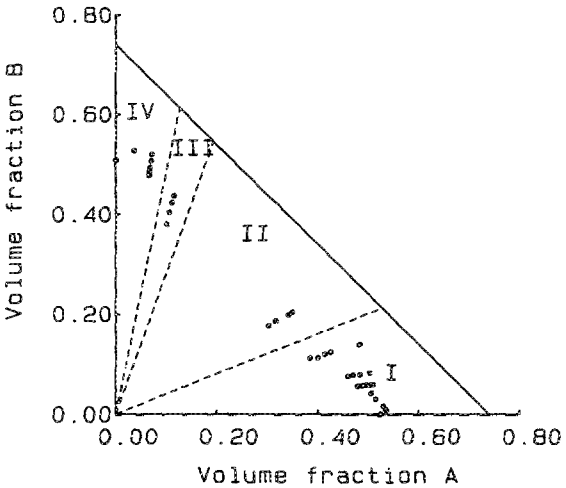

FIG. 1. A constant volume phase diagram illustrating the binary suspensions which were investigated. The phase diagram is divided into four regions (I–IV by the dotted lines) on the basis of the observed fluid/solid phase equilibria. For details, see the text.

samples of composition $x_A \geqslant 0.66$, e.g., Fig. 2(a), show it to consist of large regions of crystallinity with only a small proportion of amorphous material. By comparison, the solid phases of samples with compositions $0.43 < x_A < 0.58$, while still containing ordered regions of component A, show much larger regions of amorphous packing. A scanning electron micrograph [Fig. 2(b)] of the dried solid phase of sample 20, $x_A = 0.446$, $\varphi = 0.512$, shows that the amorphous regions contain both components A and B in the approximate composition $AB_{2.5}$. The consequence of the formation of this dense amorphous phase in samples of composition $0.43 < x_A < 0.58$ is discussed in detail in Sec. V A.

Figure 3 shows the scattered intensity profile from the solid phase of sample 59, $x_A = 0.578$, $\varphi = 0.536$. As is expected from the discussion of the previous paragraphs, this pattern is consistent with a crystal of pure A; its detailed structure will be discussed further in Sec. V B. Lattice parameters obtained from similar scattering profiles of samples with $x_A \geqslant 0.43$ are listed in Table III; they have approximate-

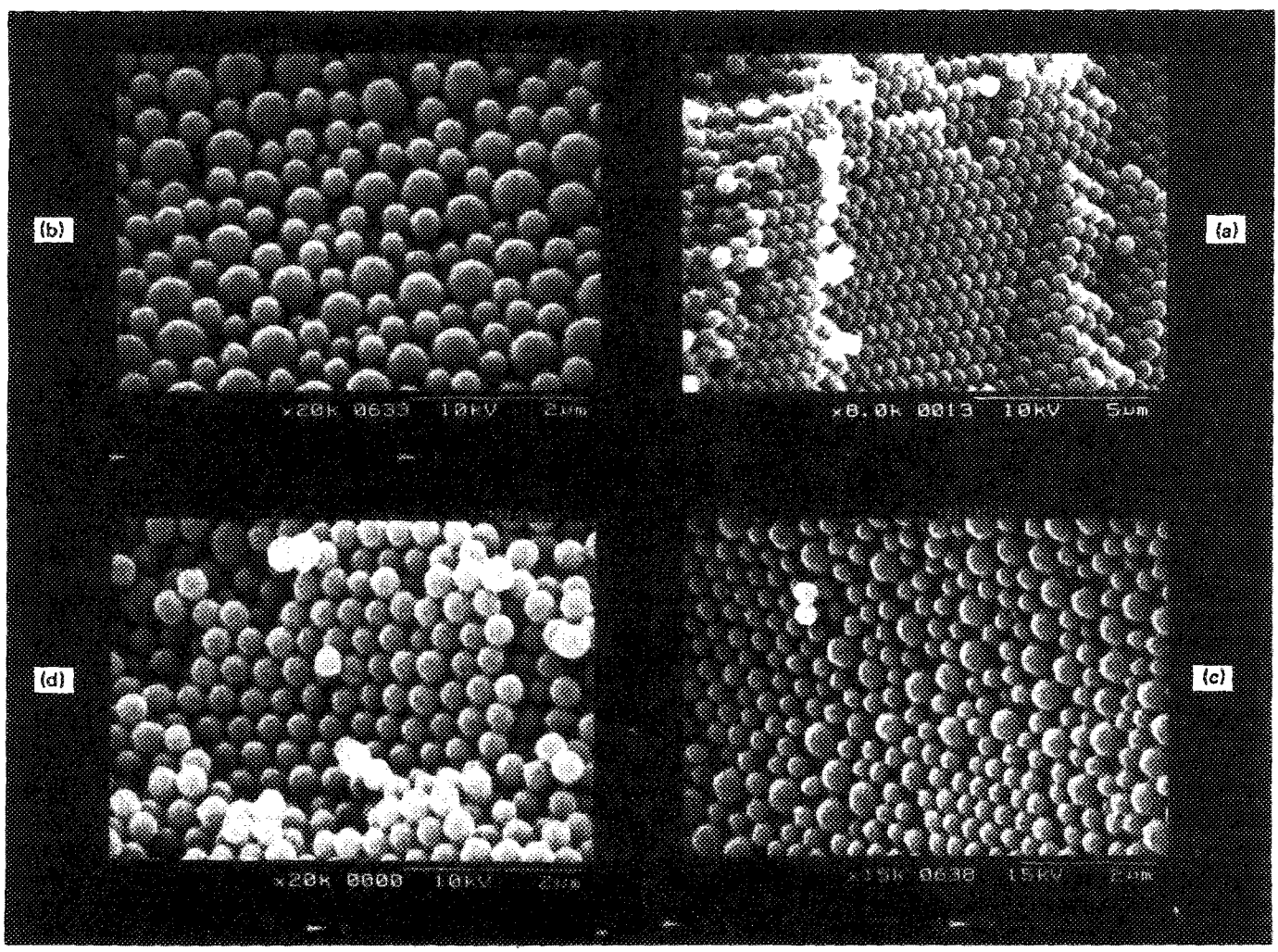

FIG. 2. Scanning electron micrographs of dried colloidal solids: (a) A crystalline region of component A formed from a suspension (sample 33) of composition $x_A = 0.660$ and volume fraction $\varphi = 0.545$. Component B has been almost totally excluded from the crystal, although the top center of the photograph shows a dissolved impurity particle of component B. (b) An example of the dense amorphous phase formed in a suspension (sample 20) of composition $x_A = 0.446$ and volume fraction $\varphi = 0.512$. The solid phase also contained highly crystalline regions of component A which are not visible in this micrograph. (c) Crystalline regions of component B and the surrounding amorphous grain boundaries found in a suspension (sample 53) of composition $x_A = 0.0563$ and volume fraction $\varphi = 0.535$. Prior to drying, this sample contained an AB_{13} crystalline phase. (d) A crystalline region containing predominantly component B formed from a suspension (sample 32) of composition $x_A = 0.0153$ and volume fraction $\varphi = 0.563$. Component A, although totally absent from the crystalline region, may be found in amorphous regions (top left-hand corner).

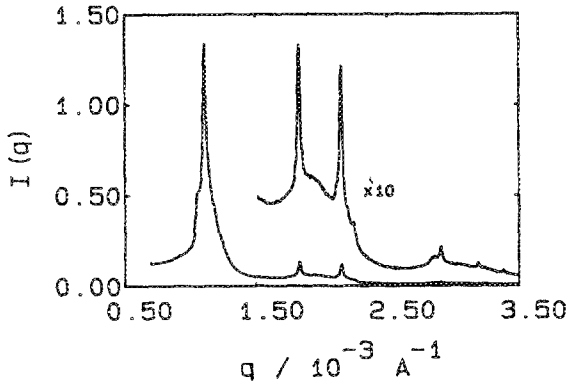

FIG. 3. The q dependence of the scattered intensity $I(q)$ in arbitrary units from the equilibrium solid phase formed from a suspension (sample 59) of number fraction $x_A = 0.578$ and volume fraction $\varphi = 0.536$. The solid phase occupied 56% of the total suspension volume. The equivalent face centered cubic lattice parameter was determined as 964 nm. As discussed in the text, the crystals were composed almost entirely of large A spheres.

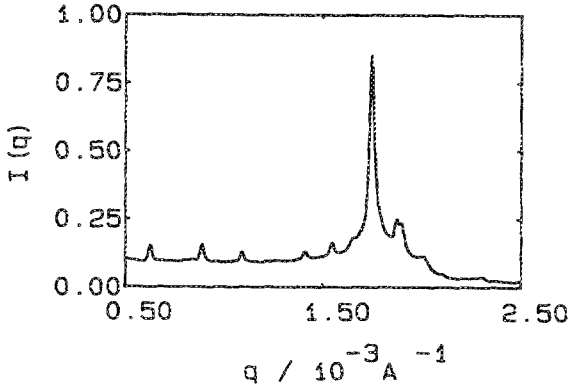

FIG. 5. The q dependence of the scattered intensity $I(q)$ in arbitrary units from the equilibrium solid phase formed from a suspension (sample 53) of number fraction $x_A = 5.63\times10^{-2}$ and volume fraction $\varphi = 0.535$. The suspension was previously slow tumbled ($\omega\sim1\times10^{-5}$ Hz) for four months. The solid sediment occupied 85% of the overall suspension volume. The scattering pattern is interpreted as arising from a mixture of crystals of pure B (causing the strong reflection at $q = 1.73\times10^{-3}$ A^{-1} and the feature at $q = 2.0\times10^{-3}$ A^{-1}) and crystals of AB_{13}.

ly the same magnitude (within 6%) as that obtained from a sample (8) of pure A, $x_A = 1$. However, closer inspection of these measured lattice parameters reveals a systematic decrease at constant overall total volume fraction φ, with decreasing number fraction x_A of component A. Similarly, in suspensions of identical composition, crystals formed in the fluid–solid coexistence region showed a decrease in lattice parameter with increasing overall total volume fraction φ. This is in contrast to the behavior observed in single component suspensions where for samples in the phase coexistence region, the lattice parameter is independent of the overall total volume fraction φ. The cause of this variation of lattice parameters is discussed in Sec. V A.

B. Region II

Four sample prepared with a number fraction $x_A \approx 0.28$ remained amorphous even after slow tumbling for many months. Figure 4 shows the scattering observed from sample 57; in contrast to Fig. 3, no sharp Bragg reflections are evident. Preliminary measurements by dynamic light scattering on samples 57 and 58 showed an essentially nondecaying component of the temporal decay of the dynamic structure factor analogous to that observed in one component colloidal glasses.[10] However, dynamic light scattering measurements on samples 55 and 56, of lower total volume fraction, were consistent with fluidlike properties. As suspensions of comparable volume fractions to samples 57 and 58, yet different compositions readily crystallized (see Table III), we associate this composition with an enhanced tendency to glass formation.

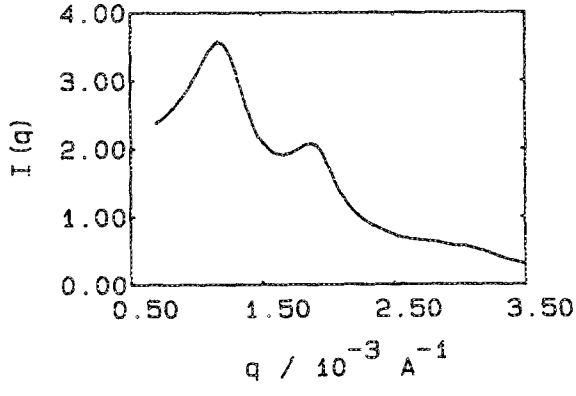

FIG. 4. The q dependence of the scattered intensity $I(q)$ in arbitrary units from the suspension (sample 57) of number fraction $x_A = 0.281$ and volume fraction $\varphi = 0.540$. The sample had been slow tumbled ($\omega\sim1\times10^{-5}$ Hz) for approximately three months. No crystallization was observed.

C. Region III

The four samples prepared with a number fraction $x_A \approx 0.057$ (approximately 16 small B spheres to one large A sphere) showed a complex sequence of phase behavior. Crystallization was first observed in suspensions of total volume fraction $\varphi = 0.511$ in which at equilibrium a single solid phase of irregularly stacked crystals of component B (for further discussion of the structure, see Sec. V B) coexisted with a fluid phase. The crystal phase showed a powder diffraction pattern similar to Fig. 6. On further increase in the volume fraction to $\varphi = 0.535$, equilibrium was observed among three phases, a binary colloidal fluid, and two solids. Measurement of the crystal powder diffraction pattern showed that initially a crystalline B phase was formed, but after slow tumbling for about four months, the scattering profile changed to that shown in Fig. 5. The diffraction pattern contained features characteristic of B crystals, but also a progression of low q reflections implying a structure with a large lattice parameter. Detailed calculations, to be published elsewhere[26] and discussed in Sec. V C, demonstrate

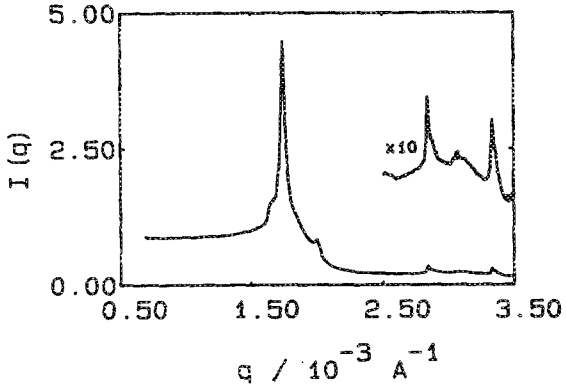

FIG. 6. The q dependence of the scattered intensity $I(q)$ in arbitrary units from the solid phase formed from a suspension (sample 64) of number fraction $x_A = 0.03$ and total volume fraction $\varphi = 0.551$. The sample was fully solid. The equivalent face-centered-cubic lattice parameter was determined as 613 nm. The crystals were composed almost entirely of small B spheres.

that the observed scattered intensity is consistent with powder diffraction from the ordered binary alloy AB_{13}. Visual observation showed that the crystallites were distributed homogeneously throughout the bulk of the cuvette. After prolonged slow tumbling ($\omega \sim 1 \times 10^{-5}$ Hz) for a total of seven months, the intensity of the low angle reflections was reduced, although they were still apparent, indicating that this AB_{13} structure may be metastable. Essentially identical phase behavior was found after the sample was shear melted by rapid ($\omega \sim 0.2$ Hz) tumbling and allowed to crystallize again under "zero gravity" conditions.

Samples of the solid phase in which light scattering measurements had indicated AB_{13} formation were dried and examined by electron microscopy. In Fig. 2(c), an electron micrograph of the dried colloidal solid phase is reproduced. A large region of crystalline component B is apparent. Although there is a high degree of short range order in the regions containing both components A and B, no examples of an ordered binary alloy structure were observed even after an extensive search. Since preparation of the sample for electron microscopy involves the removal of the suspension medium, and a consequent increase in density, one possible explanation for the absence of AB_{13} (supported by the observation of the next paragraph) is to suggest this phase although stable, or possibly metastable, at low densities is unstable at high densities.

On further increasing the volume fraction to $\varphi = 0.553$, the binary suspension totally solidified into what appeared to be a single solid phase consisting of crystals of component B. The powder diffraction pattern showed no low angle reflections and was similar to Fig. 6. No evidence was seen of a coexisting crystal phase of component A. Electron microscopy of dried colloidal solids from this sample showed ordered regions of component B with component A in amorphous grain boundaries.

D. Region IV

For $x_A \leqslant 0.05$, all samples of high enough total volume fraction solidified. The presence of a small number fraction of component A was found to reduce dramatically the rate of solidification. Figure 6 shows a typical powder diffraction pattern of the solid phase formed in this region of the phase diagram. For all samples, the measured equivalent fcc lattice parameter was comparable to the lattice parameter found for crystals of pure component B, although as in region I small systematic shifts in the lattice parameters were measurable. For example, in samples of constant number fraction x_A, the lattice parameter was observed to decrease slightly as the total volume fraction increased (see Table III).

The scanning electron micrograph of a dried solid sample, reproduced in Fig. 2(d), shows ordered regions of component B surrounded by amorphous regions consisting of both components. The solubility of component A in crystals of B appears to be negligible. In the few cases where component A was found in crystals of component B, the presence of the larger component severely perturbed the crystal structure.

IV. MODELING THE FREEZING OF BINARY COLLOIDAL HARD SPHERES

At a constant external pressure, we can treat, to a very good approximation, the total volume of the suspension (suspension medium plus colloidal particles) as constant independent of any spatial arrangement the colloidal particles may adopt. This approximation is valid because, in comparison with the compressibility of the colloidal fluid, the suspension medium is essentially incompressible. In this situation, the colloidal fluid–solid phase transition is measured under conditions of near constant volume rather than constant pressure (the usual situation in the study of metallic alloys). In multicomponent suspensions, the osmotic pressure plays a role completely analogous to that of the total pressure for a one component system. Thus the lattice parameter of the colloidal crystal is determined essentially by the suspension osmotic pressure.

We model the system by a binary mixture of hard spheres of diameter ratio α which, although miscible in the fluid phase in all proportions, are assumed to be immiscible in the crystal phase. The experimental data, discussed below, suggest this is a reasonable approximation at least for a restricted range of compositions. Detailed discussion of the model will be published elsewhere,[27] but in order to clarify the approximation used, we shall briefly summarize the approach used.

With the assumption of mutual crystal immiscibility, the phase diagram contains a fluid of eutectic composition which divides the coexisting fluid–solid boundary into two branches corresponding to the equilibrium between the fluid and crystals of component A and the fluid in equilibrium with crystals of component B. The composition of the coexisting fluid and crystals of component A, e.g., are determined by the solutions of the equations

$$T_l = T_s, \quad \Pi_l = \Pi_s, \quad (\mu_A)_l = (\mu_A)_s, \tag{3}$$

where l and s refer to the binary fluid and crystalline A phase, respectively. Accurate equations of state for both the binary hard sphere fluid[28] and the hard sphere crystal[29] are known. Both have been tested against extensive computer simula-

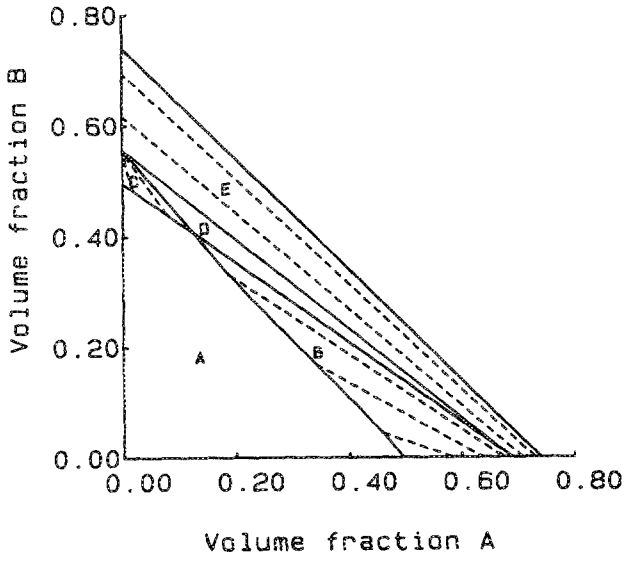

FIG. 7. The (φ_A,φ_B) projection of the phase boundaries predicted for the freezing of a binary hard sphere fluid into immiscible crystal phases. The phase diagram is calculated for a diameter ratio of 0.61. Illustrative tie lines connecting coexisting states, at constant osmotic pressure, are shown dashed in the two phase regions.

tion results.[29,30] The Helmholtz free energy F is obtained by integrating the equation of state and the chemical potentials by differentiating F; $\mu = (\partial F/\partial N)_{T,V}$. Solutions to the conditions for phase coexistence, given by equations similar to Eq. (3), may thus be found.

Figure 7 shows a projection on the (φ_A,φ_B) plane of the phase diagram for this model system. This is a convenient representation under conditions of constant volume. States of constant number fraction x_A lie on lines radiating from the origin, while states of constant total volume fraction $\varphi = \varphi_A + \varphi_B$ form lines which intersect both axes at 45°. In region (A), the binary fluid is the only stable phase, while in regions (B) and (C), the fluid is in equilibrium with a pure crystal phase. The states corresponding to the end of each tie line are the coexisting fluid and crystal phases at a defined (osmotic) pressure. Each point on the tie line corresponds to the overall composition of the initial system, which at equilibrium will phase separate into the states represented by the ends of the tie line. The relative volumes of each phase are given by the normal inverse lever rule construction. Region (D) is bounded by three vertices corresponding to the eutectic fluid composition and the volume fractions of coexisting crystalline A and B phases. Samples prepared within this region will at equilibrium phase separate into three phases of eutectic fluid and crystals of A and B. The relative volume of each phase in the eutectic region has a simple geometric interpretation in the (φ_A,φ_B) phase diagram. The volume of, e.g., the fluid phase is proportional to the area of the triangle formed by joining the point representing the overall sample composition to the two vertices which represent the remaining two coexisting phases (crystal A and crystal B). The phase rule dictates that the equilibrium (osmotic) pressure within this region is fixed. The eutectic composition for a diameter ratio of $\alpha = 0.61$ is predicted to correspond to $x_A = 0.067$, or approximately 14 small B spheres to one large A sphere. Finally, in region (E), the system has totally solidfied and crystals of A are in equilibrium with crystals of B.

A system of hard spheres will not show the complete range of phase behavior represented in Fig. 7 if the relaxation time for structural rearrangement is sufficiently long that thermodynamic equilibrium is no longer attained. At high fluid densities structural rearrangements become more difficult and at a certain density particles will be arrested in the cages formed by neighboring particles. At this point crystallization will be totally suppressed and the fluid will enter a metastable glassy state, not represented in the equilibrium phase diagram of Fig. 7. Although glasses may be formed at any composition in binary systems (at a sufficiently high density), glass formation is often found to be easiest at the eutectic composition.[31] This has been attributed to the kinetic restraints on crystal growth in a binary mixture (associated with partition of the components) which suppress nucleation at all compositions[32] together with the reduced thermodynamic driving force for homogeneous nucleation at eutectic compositions.

In classical nucleation theory,[33] the steady state homogeneous nucleation rate J is expressed in terms of a product of a transport coefficient f and a thermodynamic term associated with the free energy γ required to form a crystal–fluid interface. In a single component metastable fluid of volume fraction φ, the nucleation rate is given by

$$J = \rho f \exp\left[-\frac{16\pi\gamma^3}{3(\Delta\Pi)^2 kT}\right], \tag{4}$$

where ρ is the number density and $\Delta\Pi$ is the difference in osmotic pressure between the interior of the critical nucleus and the exterior fluid phase. The osmotic pressure difference $\Delta\Pi$ is equal to the decrease in Helmholtz free energy accompanying the formation of a unit volume of crystal at an osmotic pressure at which it will be in equilibrium with the exterior metastable fluid phase. In a fluid of constant volume fraction, the frequency factor f is expected to be largely independent of composition, while in the phase coexistence region $\Delta\Pi$ is determined primarily by the difference between the metastable and freezing fluid volume fractions. At the eutectic point corresponding to the freezing of the densest fluid, $\Delta\Pi$ will be a minimum and the thermodynamic barrier to nucleation will be at a maximum. The homogeneous nucleation rate J will thus be lowest and (in the absence of heterogeneous nucleation) a binary glass will be most readily formed in suspensions of the eutectic composition.

V. DISCUSSION

A. Comparison with immiscible sphere model

The scanning electron micrographs (Fig. 2) clearly demonstrate that a mixture of colloidal hard spheres of diameter ratio $\alpha = 0.61$ shows extended regions of solid insolubility. When a binary suspension rich in component A (region I of Fig. 1) solidifies, the phase separation results in a crystalline phase containing predominantly component A

and a fluid phase enriched in component B. In suspensions of composition $0.43 \leqslant x_A \leqslant 0.58$, a dense amorphous phase containing both A and B is also formed. The solubility of component B in the crystal of component A is negligible. The electron micrographs indicate that suspensions rich in component B (region IV) crystallize into a solid phase composed almost solely of component B. Component A is present either in amorphous grain boundaries, or separates into the binary colloidal fluid phase. There is no evidence for the formation of a substitutionally disordered crystal phase.

The measured lattice parameters for crystals in regions I and IV given in Table III are consistent with the observation of (nearly) complete solid immiscibility. The measured powder diffraction patterns of crystals formed in these regions, shown in Fig. 3 and 6, are indexed on the basis of a single crystalline phase (details of the structures are given in Sec. V B). The composition of this equilibrium crystalline phase can be deduced from the measured lattice parameter. At a constant pressure, the lattice parameter of a substitutionally disordered crystal is commonly found to vary monotonically with composition between the lattice parameters of the limiting pure crystalline phases A and B.[34] For an ideal solid solution, where the volume of mixing is assumed to be zero, the lattice parameter of the mixed crystal a_m is given by

$$a_m^3 = (1 - x_A)a_B^3 + x_A a_A^3, \tag{5}$$

where a_A and a_B refer to the lattice parameters of the pure component crystals. Lattice parameter measurements of single phase metal alloys[34] have shown that this expression is a useful first approximation relating the parameters of a solid solution to its composition. If, however, A and B are immiscible in the solid state then, at constant pressure, the lattice parameter of a single solid phase observed must correspond to either pure crystalline A or B. This last case most closely represents the data given in Table III. The small shifts in the measured lattice parameters from those of pure crystalline A or B occur since measurements are made under conditions of constant external pressure and not constant osmotic pressure.

The origin of the shift in lattice parameters is clearly seen by considering, e.g., the equilibrium between a binary fluid and a crystal phase of the larger component A. A decrease in the number fraction of A in the coexisting fluid, at a fixed volume fraction, results in an increased total particle number density and a consequent rise in osmotic pressure. The coexisting A crystals are therefore compressed and their lattice parameter reduced. The shift in lattice parameter may be predicted quantitatively by the model, described in Sec. IV, of immiscible hard sphere crystals.

The model system of immiscible hard spheres does not predict the formation of the ordered binary phase AB_{13} and therefore cannot provide a complete description of the experimental phase behavior. However, over a limited range of compositions, the predictions of this simple model are found to be in reasonable agreement with the experimental data. For suspensions rich in component A, where complete phase separation is observed, this model provides accurate predictions for experimental lattice parameters and to a lesser extent the fractional volume of the crystal phase η_s. For all the suspensions studied, the predictions of this model are listed in Table III. For ease of comparison with the experimental data, the predicted crystal density (φ_s) is expressed in terms of the equivalent fcc lattice parameter a_{calc} given by

$$a_{\text{calc}} = \left(\frac{2\pi}{3\varphi_s}\right)^{1/3} \sigma; \tag{6}$$

here σ is the hard sphere diameter, determined from light crystallography measurements on pure components and given in Table I.

For the crystalline phase in equillibrium with a binary fluid observed in region I, Fig. 8 compares the measured and predicted lattice parameters. Agreement is seen to be very close. With the decreasing number fraction x_A, the volume fraction of the crystalline phase (A) in the fluid–solid coexistence region increases markedly from $\varphi = 0.545$ for single component suspensions to volume fractions of $\varphi = 0.65$ in crystals formed from suspensions of overall composition $x_A = 0.437$. The observed reduction in the rate of crystallization as x_A decreases presumably, in part, reflects the difficulty of nucleating and growing this increasingly dense crystal phase. In sample 25 ($x_A = 0.440$), where the predicted crystal density corresponds to $\varphi = 0.68$, the rate of crystallization is sufficiently slow that the sample remained amorphous throughout our experiments and crystallization was not observed.

In Fig. 9, the predicted fractional solid volumes η_s are compared with measurements made on suspensions of a (nominally) fixed total volume fraction of $\varphi = 0.548$. In suspensions of composition $x_A \geqslant 0.66$, the agreement is seen to be close, although there seems to be a small systematic discrepancy in that the measured phase volumes are approximately 0.1 larger than the predicted values. However, much more marked deviations occur in suspensions of composition $0.43 \leqslant x_A \leqslant 0.58$. The data in Table III shows that in some suspensions within this composition band the measured solid phase volumes exceed those predicted by upwards of 0.4. For example, the model of mutually immiscible spheres predicts that at compositions identical to sample 62

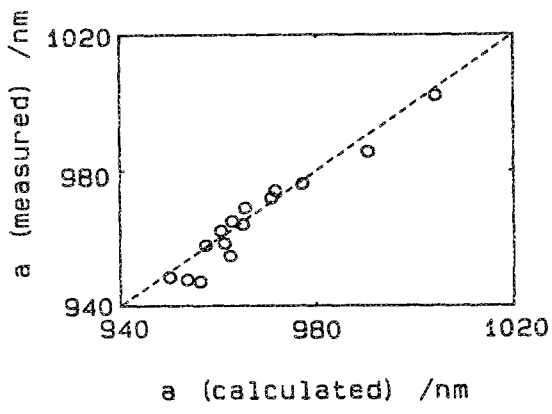

FIG. 8. Comparison between the measured lattice parameters of crystals formed from component A and those calculated from the model of immiscible spheres discussed in Sec. IV. Exact agreement between theory and experiment is shown by the dashed line.

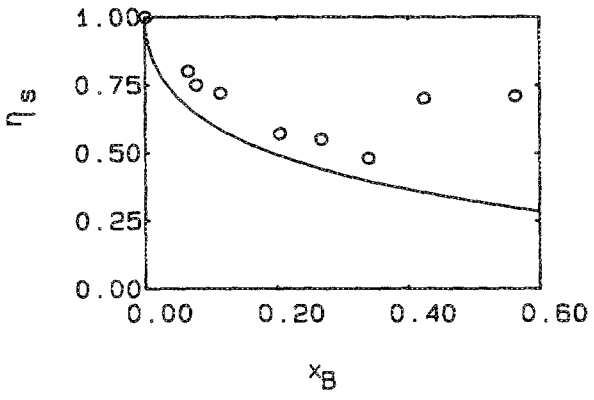

FIG. 9. The solid phase volume η_s in suspensions of total volume fraction $\varphi = 0.548 \pm 0.002$ as a function of x_B, the number fraction of small spheres ($x_B = 1 - x_A$). The solid line is the theoretical prediction of the immiscible sphere model.

about half of the sample volume will be occupied by a crystalline A phase, yet the sample was found to be fully solid. Although this discrepancy could in theory be caused by inaccuracies in the hard sphere equations of state, recent computer simulation studies for the fluid state[30] have shown only very small deviations which seem unlikely to explain the large differences observed. We suggest that the disagreement between the measured and predicted phase behavior for compositions $0.43 \leqslant x_A \leqslant 0.58$ is a consequence of the presence of an underlying phase transition. This hypothesis is consistent with electron micrographs, similar to Fig. 2(b), which show that the solid "phase" consists of ordered regions of component A and large regions of dense amorphous packing containing both components A and B. By comparison, electron micrographs of suspensions of $x_A \geqslant 0.66$, similar to Fig. 2(a), show only a relatively small amount of amorphous material mainly associated with crystal grain boundaries. The inhomogeneous nature of the solid formed in suspensions of composition $0.43 \leqslant x_A \leqslant 0.58$ suggests that, at equilibrium, crystals of component A coexist with a second crystalline phase AB_n with n as yet undetermined. Thermodynamic considerations show this postulated crystalline phase AB_n cannot be identified with the binary alloy phase AB_{13}. This suggests that at equilibrium (at least) two binary crystal phases would be formed: AB_{13} which we have observed directly and a crystal of some intermediate composition AB_n. Possible crystal structures for this intermediate binary phase are discussed further in Sec. V D.

With the presence of a second crystalline phase AB_n the equilibrium phase diagram, in the region $x_A \geqslant 0.43$, consists of two fluid–solid branches describing the equilibrium between the crystalline phases AB_n or A and a fluid phase. For suspensions richer in A than the eutectic composition, where crystals of A and AB_n both coexist with a fluid phase, the freezing densities are determined by equilibrium between crystals of A and a binary fluid. At equilibrium, the osmotic pressure (Π) and the chemical potential of component A (μ_A) is equal in both phases

$$\Pi_{(\text{fluid})} = \Pi_{(\text{crystal } A)},$$
$$\mu_{A(\text{fluid})} = \mu_{A(\text{crystal } A)}. \tag{7}$$

The phase behavior for compositions richer in B than the A-AB_n eutectic are determined by the corresponding set of equations

$$\Pi_{(\text{fluid})} = \Pi_{(\text{crystal } AB_n)},$$
$$\mu_{A(\text{fluid})} = \mu_{A(\text{crystal } AB_n)},$$
$$\mu_{B(\text{fluid})} = \mu_{B(\text{crystal } AB_n)}. \tag{8}$$

In the three phase eutectic region, Eqs. (7) and (8) must be simultaneously satisfied. Equation (7) is identical with those solved in the model of mutual immiscible spheres discussed in Sec. IV. The only influence of the second crystalline phase AB_n is to limit the range of densities over which Eq. (7) solely determine the phase behavior. Therefore samples in which the experimental phase volumes (or lattice parameters) deviate markedly from the model predictions, given above, must at equilibrium consist of, at least partially, AB_n crystals. Hence, assuming the presence of the crystalline phase AB_n, the suspensions prepared with compositions $0.43 \leqslant x_A \leqslant 0.58$ are not at equilibrium, but in some long lived, probably metastable state.

Finally it should be noted that for the slow rates of crystallization observed in these experiments, the slow rotational tumbling used to reduce gravitational settling may possibly influence the phase behavior. Since at present there seems no practical alternative to slow tumbling, it seems simplest to discuss our findings in terms of an assumed equilibrium phase behavior.

B. Structure of the phase separated crystals

The powder diffraction patterns of crystals formed in regions I and IV of the phase diagram (Figs. 3 and 6) show a combination of sharp Bragg diffraction peaks and a structured, but diffuse background. Similar diffraction patterns have been observed for single component colloidal crystals[17] and have been interpreted as diffraction from a randomly orientated powder of disordered close packed crystals. The crystal structure postulated may be physically realized by the irregular stacking of nearly perfect hexagonal planes of spheres. Selecting hexagonal basis vectors ($\mathbf{a}$,$\mathbf{b}$) in the reference plane, a close packed arrangement of planes is generated by successive layers which are displaced by a translation perpendicular to the plane (along the c axis) and by the translations $(2\mathbf{a} + \mathbf{b})/3$ or $(\mathbf{a} + 2\mathbf{b})/3$ in the plane. The three different plane positions obtained by these translations may be designated by A, B, or C. In a close packed structure, any particular layer is always followed by a layer of a different kind. The two simplest periodic close packed structures—hexagonal close packed and face centered cubic—differ in the arrangement of second neighboring planes; in hexagonal packing, they are of the same kind and the plane arrangement is, e.g., $ABABAB\ldots$, while in face centered cubic, the plane sequence is $ABCABC\ldots$ and second neighboring planes always differ. In Ref. 17, the powder pattern is calculated for close packed structures in which a degree of randomness is assumed in the choice of second neighboring

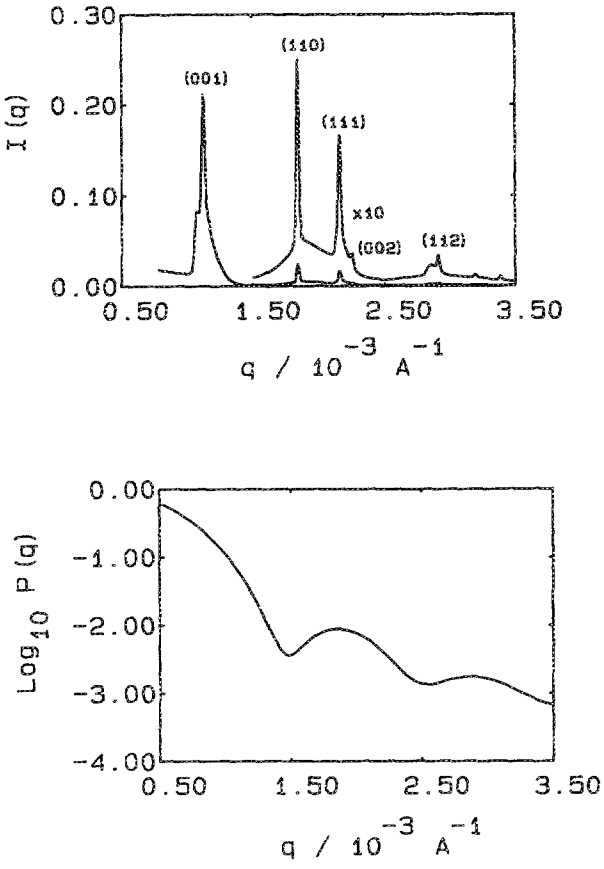

FIG. 10. (a) The calculated powder diffraction pattern $I(q)$ in arbitrary units of an irregularly stacked close packed crystal of component A. The lines are indexed on a hexagonal basis (with lattice vector c having length equal to the interplane spacing). A stacking parameter β of 0.6 was used. (b) The particle form factor $P(q)$. It was determined from measurements made on a dilute single component suspension with a medium refractive index close to that of sample 59.

planes, the probability of different second neighboring planes being defined as β. Reflections from planes (hkl) where $h-k=0 \pmod 3$ are unaffected by an arbitary value of β and remain sharp, while reflections where $h-k \neq 0 \pmod 3$ are broadened to produce a diffuse background.[35]

The angular intensity of scattered light $I(q)$ from a randomly orientated powder of crystallites consisting of identical spherical particles is proportional to the product of the particle form factor $P(q)$ and the orientationally averaged crystal structure factor $S(q)$. The particle form factor $P(q)$ is the Fourier transform of the volume polarizibility profile of the particle and is determined by the size, shape, and refractive index of internal features throughout the particle. The structure factor $S(q)$ is the orientational average of the Fourier transform of the equilibrium density autocorrelation function and is therefore a measure of the correlation between the positions of particles within a crystal. Figure 10 shows the calculated intensity $I(q)$ for a random powder of close packed crystals consisting solely of component A, where the stacking parameter has been taken as $\beta = 0.6$. The orientationally averaged crystal structure factor $S(q)$ was calculated by methods described elsewhere,[17] while the particle form factor $P(q)$, shown in Fig. 10(G), was determined from the measured intensity $I(q)$ of dilute dispersions where $S(q)$ may be assumed to be unity. Comparison with the experimental data in Fig. 3 shows that the calculated powder diffraction pattern faithfully reproduces the bands of diffuse scattering around each Bragg peak even for high order reflections. Much of the discrepancy between the calculated and observed intensities is probably due to the use of an inaccurate form factor which, near refractive index match, is very sensitive to experimental conditions. Similar values for the stacking parameter β have been obtained from single component crystals[17] and consequently the crystal structure in the binary dispersions seems to be relatively unaffected by phase separation.

C. Binary alloy formation

A full discussion of the structure and requirements for binary alloy formation will be given in a subsequent report,[26] but for completeness, we summarize our observations. In a restricted range of volume fractions, suspensions of number fraction $x_A = 0.057$ containing approximately 16 small B spheres to one large A sphere showed binary alloy formation. The observed diffraction pattern (Fig. 5) of the solid phase contained features characteristic of pure B crystals and also a regular progression of low q reflections implying a structure with a large lattice parameter. Detailed calculation demonstrates that the observed scattering intensity is reproduced by powder diffraction from the ordered binary alloy AB_{13}. The structure of this compound can be considered in terms of a simple cubic subcell with A spheres at the cube corners. The cube contains a body-centered B sphere surrounded by 12 nearest neighboring B spheres at the vertices of a regular icosahedron. The cubic unit cell is constructed from eight subcells with each adjacent icosahedral cluster rotated by $\pi/2$ about a simple cubic axis. A similar structure is found in the intermetallic compound $NaZn_{13}$, although the internal cluster of Zn atoms is slightly distorted from a regular icosahedral geometry.[36]

D. Comparison with previous calculations

Thermodynamic phase diagrams for mixtures of hard spheres of arbitrary diameter ratio have recently been calculated by Haymet and co-workers.[5] The first order phase transition was treated by a density functional theory of freezing in which the correlation function of the crystal was approximated, using thermodynamic perturbation theory, by the correlation function of the coexisting liquid. The lattice symmetry must be assumed and a variety of symmetries tested to find the most stable crystal. The density functional theory is not an exact description of freezing but, at least for single component systems,[37] its predictions are in reasonable agreement with essentially exact computer simulation results. Rick and Haymet[5] have considered the freezing of hard sphere mixtures of equal number fraction ($x_A = 0.5$) for which they conclude the stable solid phase at all size ratios is the substitutionally disordered fcc structure. Meta-

stable solutions were found for the other crystal symmetries considered of CsCl, NaCl, and a "fast sphere" phase in which the big spheres are frozen in a fcc lattice, while the small spheres are translationally disordered. In our experiments, we do not observe formation of a substitutionally disordered crystal at any composition. The discussion above suggests that at equilibrium (colloidal) mixtures of composition $x_A = 0.5$ will initially freeze either into crystals of A and a fluid phase, crystals of AB_n and a fluid phase, or into a three phase eutectic region of coexisting A, AB_n, and fluid depending upon the exact position of the eutectic. In part, this disagreement between our results and the density functional calculations may be ascribed to the rather limited set of crystal symmetries considered in the calculations so far. The discussion below suggests that for a size ratio of $\alpha = 0.61$, the most important crystal symmetries are probably aluminium diboride (AB_2) and the regular icosahedral $NaZn_{13}$ structure (AB_{13}). To the best of our knowledge, no calculation which includes the possibility of freezing into these structures has been reported.

It is interesting to compare our results with the packing predictions of Sanders and Murray.[4] In their calculations of mixtures of hard spheres they assumed entropic terms could be ignored, so that the phase behavior was determined purely by geometric factors. In this approach, a mixture of hard spheres was assumed to freeze into a structure which maximized the total packing fraction. Unfortunately, even for a specified diameter ratio, no means exist to determine the structures which maximize the total packing fraction. The only route available is to test a variety of common crystallographic structures. Murray and Sanders considered a range of binary structures based on cubic or hexagonal packing. For diameter ratios $0.482 < \alpha < 0.624$, only an AB_2 arrangement based on the crystallographic aluminium diboride structure was found with a packing fraction greater than the phase separated close packed crystals of A and B ($\varphi = 0.7405$). The ideal cubic phase AB_{13} cannot have a packing fraction greater than 0.738. Hence, spheres of diameter ratio $0.482 < \alpha < 0.624$ are likely to freeze into an AB_2 phase together with either crystals of A or B depending upon the overall composition. However, Murray and Sanders further showed that, with a small modification to the ideal structure of AB_{13}, the packing density could be increased so that AB_{13} was marginally preferred to the close packed crystals of A or B. The expressions given by Murray and Sanders predict, for a diameter ratio of $\alpha = 0.61$, the maximum packing density of the AB_2 structure as $\varphi = 0.750$, while the ideal AB_{13} structure has a maximum density of $\varphi = 0.685$. Even allowing a slight deviation from the ideal icosahedral structure of AB_{13}, the maximum density of $\varphi = 0.714$ is still below the close packed limit for monodisperse spheres. Hence, for diameter ratio $\alpha = 0.61$, the AB_{13} structure is predicted by these arguments to be unstable with respect to a phase separation into AB_2 and B.

Comparison of the predictions of Murray and Sanders with our results show a remarkably close correspondence if we identify the (hypothesized) phase AB_n with AB_2. The crystal AB_2 consists of layers of B spheres in planar hexagonal rings, similar to the carbon layers in graphite, alternating with close packed layers of A spheres. Nucleation and growth of this structure, with its alternating layers of spheres, seems likely to be very slow and easily disrupted by the inclusion of a different sized sphere into a growing plane. This may account for the (metastable) amorphous phases observed in suspensions of composition $0.43 \leqslant x_A \leqslant 0.58$ and explain the absence of any crystalline AB_2 phase. In agreement with the predictions of Murray and Sanders, the experimental observations suggest the AB_{13} phase was probably metastable. The relatively easy formation of AB_{13} in contrast to the absence of the (hypothesized) phase AB_2 may in part reflect the importance of local isocahedral structures in dense liquids.

VI. CONCLUSIONS AND SUMMARY

With increasing concentration, a binary mixture of (colloidal) hard spheres must either form a glass or freeze into one of three distinct types of crystalline solids: (1) a pure component crystal; or (2) an ordered binary crystal where each component lies on a crystalline sublattice; or (3) a substitutionally disordered binary crystal in which each colloidal component is distributed with only short range order on a common lattice. We have studied the fluid–solid transition in suspensions of colloidal hard spheres of relative diameter $\alpha = 0.61$ as a function of suspension volume fraction and composition. Although for this size ratio there is no evidence for the formation of substitutionally disordered crystals, colloidal hard spheres show examples of each of the three remaining classes of solids.

The observed solid phases are determined principally by the number fraction x_A of the larger colloidal component (labeled A) in the suspension. In limited regions of composition, either close to suspensions of pure A ($0.66 \leqslant x_A \leqslant 1.00$) or pure B ($0 \leqslant x_A \leqslant 0.057$), the two components show (almost) complete solid immiscibility and only crystals of each pure component are formed. In this range of compositions, binary suspensions, at concentrations between freezing and melting, froze with phase separation into a pure component crystalline phase and a coexisting fluid phase enriched in the noncrystallizing component. Suspensions of composition $0.43 \leqslant x_A \leqslant 0.58$ showed a slightly different set of phase behavior. At concentrations between freezing and melting, suspensions similarly froze into crystals of pure A, but the samples also contained an additional dense amorphous phase of approximate composition $AB_{2.5}$. Suspensions prepared with approximately the same overall composition ($x_A \approx 0.28$) did not crystallize at all during the course of our experiments. Dynamic light scattering suggested that the samples had formed binary glasses. With a further increase in the proportion of small spheres, the freezing phase behavior changed dramatically. Suspensions of composition $x_A = 0.057$ (approximately AB_{16}) froze in a narrow band of concentrations, between freezing and melting, into the ordered binary crystal phase AB_{13}. In suspensions of $\varphi = 0.535$, the binary phase AB_{13} was found coexisting with crystals of pure B and a binary fluid phase. However, there were indications that the AB_{13} structure was probably metastable.

Our results show that a binary fluid of (colloidal) hard spheres exhibits a remarkably varied set of freezing behavior. The complexity of the phase behavior suggests that a theoretical description of the complete phase diagram will be difficult. However, a simple model of solid immiscible hard spheres provides accurate predictions at least for compositions approaching either the pure A or pure B limits. The system is modeled by a binary mixture of hard spheres which, although completely miscible in the fluid phase, are assumed to be mutually immiscible in any solid phase. The conditions for phase coexistence may be derived from accurate equations of state available for both the binary hard sphere fluid[28] and the hard sphere crystal.[29] For suspensions of composition $x_A \geqslant 0.66$, which at equilibrium phase separate into crystals of pure A and the coexisting fluid, the predictions are in good agreement with both the measured crystal lattice parameters (and hence the density of the crystal) and the volume of the coexisting crystal phase. However, in suspensions of composition $0.43 \leqslant x_A \leqslant 0.58$, a discrepancy is found between measured and predicted crystalline phase volumes. We suggest this disagreement may signify the presence of an underlying phase transition. In that case, the dense amorphous phase, which is found coexisting in these samples with crystals of A, will at equilibrium crystallize into a new binary crystal phase AB_n. Calculation of the maximum packing densities for a range of crystal structures based on hexagonal or cubic packing suggest the most probable crystalline phase is the crystallographic aluminium diboride structure AB_2.

Our results demonstrate that a binary fluid can freeze into any one of at least three different crystal phases A, AB_{13}, and B depending upon the suspension composition. It seems likely therefore that the equilibrium phase diagram will contain (at least) two eutectic regions corresponding to the solid phase separation between crystal compositions A, AB_{13}, and B. Although our data is not sufficiently detailed to completely determine the phase diagram, we have at least observed phase behavior qualitatively consistent with a eutectic region between AB_{13} and B. Suspensions of composition $x_A = 0.057$, at a concentration just above freezing ($\varphi = 0.511$, sample 52) separated into crystals of B and a coexisting fluid (two phase fluid–solid region). With a concentration increased to $\varphi = 0.535$ (sample 53), the suspension froze into AB_{13}, B, and a coexisting fluid as expected for compositions within the three phase eutectic region. With a further increase in density to above the melting concentration, the suspension is expected to completely freeze into two coexisting solid phases of AB_{13} and B. In partial agreement with this, in sample 54 ($\varphi = 0.553$) no fluid phase was found, although the only crystalline phase observed was B. Presumably the relatively small volume of A spheres remained in amorphous phases which at equilibrium will crystallize into AB_{13}.

Our results illustrate the wide range of both equilibrium and metastable crystal structures which can be formed by mixtures of (colloidal) hard spheres, where only packing considerations are significant. In atomic and molecular systems, by contrast, the enormous variety of crystalline structures is dictated as much by molecular geometry and electronic properties as by repulsive forces. Comparison between the crystal structures of hard spheres and atomic and molecular systems offer the possibility of assessing the relative importance of these various factors in determining the stable crystal structures.

ACKNOWLEDGMENTS

We are grateful to Professor D. W. Oxtoby for a number of helpful comments and suggestions. We would also like to thank S. Papworth for the synthesis and characterization of the polymer particles.

[1] J. P. Hansen and I. R. McDonald, *Theory of Simple Liquids*, (Academic, London, 1976).
[2] B. J. Alder, J. Chem. Phys. **40**, 2724 (1964); J. L. Lebowitz and J. S. Rowlinson, *ibid.* **41**, 133 (1964).
[3] J. L. Barrat, M. Baus, and J. P. Hansen, J. Phys. C **20**, 1413 (1987).
[4] J. V. Sanders and M. J. Murray, Philos. Mag. **42**, 721 (1980).
[5] S. W. Rick and A. D. J. Haymet, J. Chem. Phys. **90**, 1188 (1989).
[6] D. L. Ermak, B. J. Alder, and L. R. Pratt, J. Phys. Chem. **85**, 3221 (1981).
[7] W. G. McMillan and J. E. Mayer, J. Chem. Phys. **13**, 276 (1945).
[8] J. G. Kirkwood and F. P. Buff, J. Chem. Phys. **19**, 774 (1951).
[9] L. Antl, J. W. Goodwin, R. D. Hill, R. H. Ottewill, S. M. Owens, S. Papworth, and J. A. Waters, Colloid Surf. **17**, 67 (1986).
[10] P. N. Pusey and W. van Megen, Phys. Rev. Lett. **59**, 2083 (1987).
[11] B. J. Ackerson and P. N. Pusey, Phys. Rev. Lett. **61**, 1033 (1988).
[12] S. Yoshimura and S. Hachisu, Prog. Colloid Polymer Sci. **68**, 59 (1983).
[13] R. J. Cairns, R. H. Ottewill, D. W. Osmond, and I. Wagstaff, J. Colloid Interface Sci. **54**, 45 (1976).
[14] I. Livsey and R. H. Ottewill, Colloid Polymer Sci. **267**, 421 (1989).
[15] P. N. Pusey and W. van Megen, Nature **320**, 340 (1986).
[16] I. Markovic, R. H. Ottewill, S. M. Underwood, and Th. F. Tadros, Langmuir **2**, 625 (1986).
[17] P. N. Pusey, W. van Megen, P. Bartlett, B. J. Ackerson, J. G. Rarity, and S. M. Underwood, Phys. Rev. Lett. **63**, 2753 (1989).
[18] P. G. de Gennes, Adv. Colloid Interface Sci. **27**, 189 (1987).
[19] H. J. Taunton, C. Toprakcioglu, L. J. Fetters, and J. Klein, Nature **332**, 712 (1988).
[20] D. Frenkel and A. J. Ladd, J. Chem. Phys. **81**, 3188 (1984).
[21] P. N. Pusey and W. van Megen, J. Chem. Phys. **80**, 3513 (1984).
[22] R. H. Ottewill and I. Livsey, Polymer **28**, 109 (1987).
[23] A. K. van Helden and A. Vrij, J. Colloid. Interface Sci. **76**, 418 (1980).
[24] W. G. Hoover and F. H. Ree, J. Chem. Phys. **49**, 3609 (1968).
[25] K. E. Davis and W. B. Russel, Adv. Ceramics **21**, 573 (1987); K. E. Davis, W. B. Russel, and W. J. Glantschnig, Science **245**, 507 (1989).
[26] P. Bartlett, R. H. Ottewill and P. N. Pusey (in preparation).
[27] P. Bartlett, J. Phys. C (in press).
[28] G. A. Mansoori, N. F. Carnahan, K. E. Starling, and T. W. Leland, J. Chem. Phys. **54**, 1523 (1971).
[29] D. A. Young and B. J. Alder, J. Chem. Phys. **70**, 473 (1979).
[30] G. Jackson, J. S. Rowlinson, and F. van Swol, J. Phys. Chem. **91**, 4907 (1987).
[31] M. H. Cohen and D. Turnbull, Nature **189**, 131 (1961).
[32] F. Spaepen and D. Turnbull, Annu. Rev. Phys. Chem. **35**, 241 (1984).
[33] D. Turnbull and J. C. Fisher, J. Chem. Phys. **17**, 71 (1949).
[34] W. B. Pearson, *Handbook of Lattice Spacings and Structure of Metals and Alloys* (Pergamon, London, 1958).
[35] A. Guinier, *X-ray Diffraction in Crystals, Imperfect Crystals, and Amorphous Bodies* (Freeman, San Francisco, 1963).
[36] D. P. Shoemaker, R. E. Marsh, F. J. Ewing, and L. Pauling, Act. Crystallogr. **5**, 637 (1952).
[37] A. D. J. Haymet and D. W. Oxtoby, J. Chem. Phys. **84**, 1769 (1986).